BIOMICROFLUIDICS **10**, 043507 (2016)

Extra dissipation and flow uniformization due to elastic instabilities of shear-thinning polymer solutions in model porous media

Anaïs Machado,[1] Hugues Bodiguel,[2,a)] Julien Beaumont,[1] Gérald Clisson,[1] and Annie Colin[3]
[1]*Univ. Bordeaux, CNRS, Solvay, Lab. LOF UMR5258, Pessac, France*
[2]*Univ. Grenoble Alpes, CNRS, Lab. LRP UMR5520, F-38000 Grenoble, France*
[3]*ESPCI, SIMM UMR 7615, 11 rue Vauquelin, 75005 Paris, France*

(Received 18 February 2016; accepted 13 June 2016; published online 5 July 2016)

We study flows of hydrolized polyacrylamide solutions in two dimensional porous media made using microfluidics, for which elastic effects are dominant. We focus on semi-dilute solutions (0.1%–0.4%) which exhibit a strong shear thinning behavior. We systematically measure the pressure drop and find that the effective permeability is dramatically higher than predicted when the Weissenberg number is greater than about 10. Observations of the streamlines of the flow reveal that this effect coincides with the onset of elastic instabilities. Moreover, and importantly for applications, we show using local measurements that the mean flow is modified: it appears to be more uniform at high Weissenberg number than for Newtonian fluids. These observations are compared and discussed using pore network simulations, which account for the effect of disorder and shear thinning on the flow properties. *Published by AIP Publishing*. [http://dx.doi.org/10.1063/1.4954813]

I. INTRODUCTION

Flow in porous media is encountered in a wide variety of applications and of natural phenomena, from chemical engineering to soil science. Usually, Reynolds numbers are small in porous media due to the small length scales involved, and flows are laminar and dominated by viscous forces. In some applications, as for enhanced oil recovery but also for soil remediation, complex fluids such as polymer solutions are used to obtain a better control of the flow. The primary interest of using polymer solutions is to increase the viscosity of the fluids, in order to limit fingering phenomena occurring in biphasic flows.[1–3]

This is usually achieved by using long polymer chains, where a large viscosity increase may be obtained with only a small amount of polymer. However, these solutions behave very differently to Newtonian fluids. They exhibit shear-tinning properties,[4] viscoelastic behavior,[5] and slippage at the wall.[6–8] Above the overlap concentration and for sufficiently high flow rates, elasticity and shear-thinning become very important. As a consequence, elastic forces dominate viscous ones. The balance between these two is given by the Weissenberg Number, $\mathrm{Wi} = N_1/2\sigma$, where N_1 is the first normal stress difference, and σ is the shear stress. When Wi exceeds some critical value which depends on the flow geometry, elastic instabilities appear.[9–12] These instabilities may evolve towards turbulence,[13] even in the limit of vanishing Reynolds numbers. In the context of flows in porous media where inertia is negligible, flows of elastic liquids might be used to trigger turbulence, which may be beneficial, in terms of mixing, for example.[14]

Recently, direct observations of elastic instabilities in two-dimensional models of porous media made using microfluidics have been reported.[15,16] It is shown in these works that the streamlines exhibit fluctuations at high enough flow rates. Above the threshold, the apparent diffusion coefficient is greatly enhanced,[16] the apparent viscosity is increased,[15,17] and some

a)Electronic mail: hugues.bodiguel@univ-grenoble-alpes.fr

trapped oil droplets are mobilized.[15,18] This last consequence is likely to be related to oil field results in Wang,[19,20] where additional oil has been recovered using polymer flooding in the semi-dilute regime. Clarke *et al*. proposed that oil mobilization is related to pressure fluctuations, which has been recently confirmed in three-dimensional structures.[21]

The question of the role of viscoelasticity in flows of porous media has been the focus of numerous studies since the 1960s (see pioneer work in Refs. 22–24). The increase in the pressure drop at high Wi numbers has been discussed (see, for example, Ref. 25) as related to extensional flows as the fluid flows through contractions.[26] However, more recent experimental results[27] in model geometries indicate that the succession of converging/diverging flows has little effect on the pressure gradient as compared to the curvature of the streamlines which promote unsteady flows. Generally speaking, the general description of flow of viscoelastic liquids in porous media remains an open issue (see, for example, Ref. 28 and references therein). For example, one might wonder about the role of disorder of the porous structure, as the model porous media used in Refs. 15 and 16 are periodical and the streamlines of the base flow exhibit a well defined curvature. Another issue is related to the role of the strong shear-thinning properties of the polymer solutions. In some systems, shear-thinning is so important that the shear stress σ increases only slightly with the shear rate $\dot{\gamma}$: for example, in semi-dilute solutions of hydrolized polyacrylamide (HPAM) used in petroleum engineering, $\sigma \sim \dot{\gamma}^{0.2}$ in some shear rates ranges.[29] In a previous communication, we reported that shear-thinning coupled to elastic instabilities in straight channels leads to a decrease in the apparent viscosity as compared to the bulk,[29] above Wi $\sim$ 5. This is in apparent contradiction with the extra dissipation due to elastic instabilities found in cone and plate geometry[5] and in porous media.[15,17]

In this work, we report a comprehensive study dealing with the flow of shear-thinning polymer solutions in model porous media. The polymer solutions are characterized by classical rheological measurements in cone and plate geometries. Taking advantage of microfluidics, we design specific porous media: an array of straight channel and a network of channels having heterogeneous widths. The use of porous media micromodels of well defined geometry and disorder allows us to perform pore network simulations on the same geometry and to compare to experiments. These simulations do not include viscoelasticity but only shear-tinning. They thus serve as a reference for low Weissenberg numbers. In the porous medium micromodel, experimental results show, similarly to previous studies, an increase in the pressure drop at high Wi numbers. We also observe a smaller increase in the pressure drop in straight channels, for higher Wi than in Ref. 29, which resolves the above mentioned apparent contradiction. Local observations reveal the existence of elastic instabilities in this range of Wi. The interplay between the shear-thinning property of the polymer solutions, the elastic instabilities, the geometry of the porous media, and the heterogeneities of the flow in the porous media are highlighted and discussed. In particular, we show that the tortuosity, which is usually defined as the relative mean length of the streamlines, depends on the shear-thinning properties of the polymer solutions for laminar flow, and not only on the structure of the porous medium. Above the onset of elastic instabilities, experimental data show that the effective tortuosity is increased and eventually becomes greater than that of a Newtonian fluid. The values of the critical Weissenberg numbers are discussed in this framework. The main originality of our work is to address the role of shear thinning on the instability.

The manuscript is organized as follows. The first section deals with the preparation of the microfluidic devices and the measurements of the rheological properties. In a second section, we detail the numerical methods and results. The third section details the experimental measurements and their analysis. The last section is devoted to the conclusion.

II. MATERIALS AND METHODS

A. Device and setup

In this work, we use two mcirofluidic devices made of SU8 resin (Microchem 3100 series), using photolithography. The fabrication procedure has been described in Ref. 4. The first device is a micromodel of a porous medium. It consists of a channel network of heterogeneous widths,

arranged in a square lattice. The lattice is orientated along the flow direction, allowing the distinction between channels parallel to the flow with those perpendicular to the flow. The height h of the channels is uniform and equal to 67 μm. The width of each channel is set randomly according to a log-normal distribution of mean value $w = 30\,\mu$m and of standard deviation $\Delta w = 10\,\mu$m. In the following, we refer to the relative standard deviation $\epsilon = \Delta w/w$ which equals 0.33. The network is made of $N = 160$ perpendicular channels and 40 parallel ones. The wavelength of the lattice is 250 μm, in both parallel and transverse directions. The porosity is 0.24. The total dimension of the porous domain is 1×4 cm. In the inlet and outlet, we added a wide cell empty of pillars, made to reduce end effects. Fig. 1 displays the mask used for the photolithography procedure, and a magnified image of the device, obtained before bonding.

The second device used is made of an array of 40 identical parallel channels. This device shares the same global features as the porous medium micromodel: length (4 cm), channel width (30 μm), inlet, and outlet. The height of this device is 45 μm. This second device has been used as a reference for pressure drop measurements.

The devices are connected to a syringe pump (Nemesys) which injects the fluids at a constant flow rate. The range of flow rates investigated is from 5 to 1000 μl/h. Next to the inlet and the outlet, we connect pressure sensors (Honeywell, ASDX 30 psi), which allows us to record the pressure drop at a frequency of 1 Hz. For a given flow rate, after a transient regime, the pressure drop stabilizes and we systematically average its value at steady state. Depending on the flow rates, the duration of the transient regime could be as long as 30 min.

B. Rheological properties

We investigated two solutions of hydrolyzed polyacrylamide (HPAM) of molecular weight 18×10^6 g/mol, obtained from SNF (3630 s). The polymer is dissolved in pure water, at concentrations of 0.1% and 0.4% in weight.

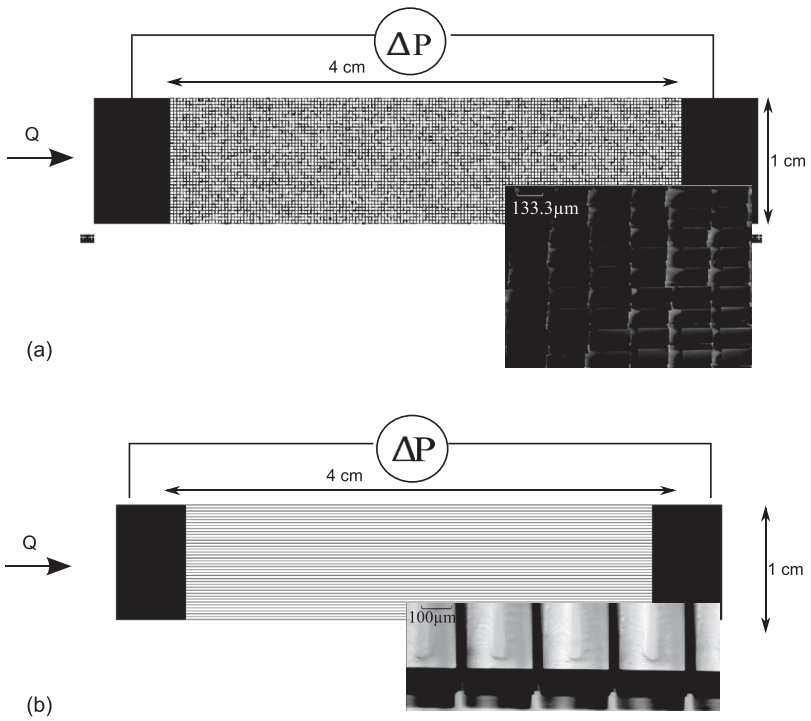

FIG. 1. Images of the masks used to manufacture the micromodel of porous medium (top) and the array of parallel channels (bottom). In inset, top, is shown a TEM image of few nodes of the porous media. The mean width of the channel is 30 μm, and the height is 67 μm. In inset bottom, optical picture of the entrance of the channels in the array of parallel channels (width 30 μm and height 45 μm).

We performed global rheological measurements using a stress-controlled rheometer (TA instruments ARG2) that can also impose a fixed shear rate using a feedback loop. We used a cone-and-plate geometry with sanded surfaces of diameter 40 mm and angle 1°. A solvent trap is used to prevent evaporation. The temperature was fixed at 20°.

The results are plotted in Fig. 2. The two HPAM solutions exhibit a strong shear thinning behavior over the whole range of shear rates $\dot{\gamma}$ investigated. For both concentrations, the shear stress σ is well approximated by a power law function $\sigma = K\dot{\gamma}^n$, and the value of n is about 0.2. We emphasize that this is a rather low value. At low shear rates, the data deviate from the power law function, but these low shear rates are out of the range of the experiments in the microfluidic device. At high shear rates, and especially for the 0.1% solution, the apparent shear stress is higher than the extrapolation of the power law function. This is likely to be due to some elastic instabilities (see below), as we observe that for shear rates greater than $50\,s^{-1}$, the instantaneous shear stress exhibits significant fluctuations.

Using simultaneous normal force measurements, we compute the Weissenberg Number, which we define as $\mathrm{Wi} = N_1/2\sigma$, where N_1 is the first normal stress difference. As highlighted in Refs. 5 and 29, it is important to define the Weissenberg number from non-linear properties rather than the linear relaxation time, which is sometimes used, as it is much higher and not relevant to the flow in the shear-thinning regime. The results are plotted in Fig. 2. The

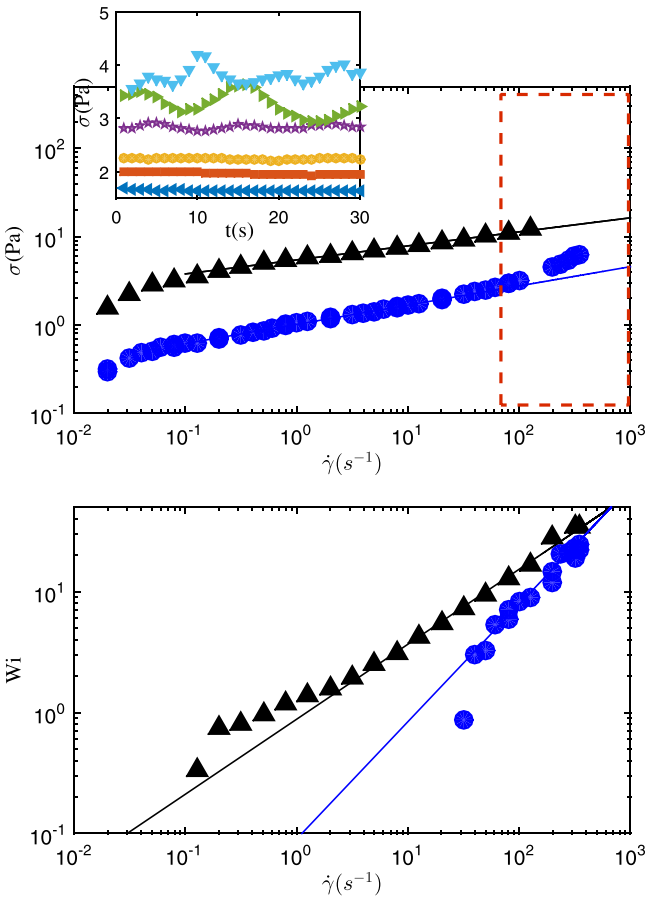

FIG. 2. Top: wall shear stress as a function of shear rate. Results obtained in cone and plate geometry at imposed shear rate for the 0.4% (△) and 0.1% solutions (○). The straight lines are the best power-law fits to the data. They are given by $5.46 \times \dot{\gamma}^{0.16}$ (0.4 wt. %) and $1.02\dot{\gamma}^{0.22}$ (0.1 wt. %). Bottom: Weissenberg number versus shear rate. The Weissenberg numbers follow power-law functions of the shear rate that are given by: $0.09\dot{\gamma}^{0.97}$ (0.1 wt. %) and $0.88 \times \dot{\gamma}^{0.62}$ (0.4 wt. %). The inset displays the transient measurements of the shear stress for several shear rates applied: (from bottom to top) 10, 20, 50, 80, 100, and $200\,s^{-1}$. Important fluctuations are observed for the three highest shear rates. These indicate that in the range of shear rate delimited by the dashed rectangle, the flow in unstable in the cone-and-plate geometry.

Weissenberg number exhibits a power law variation with respect to the shear rate, at least in the range of shear rates where we performed the microfluidics experiments. We find that $\mathrm{Wi} = 0.09\dot{\gamma}^{0.97}$ for the 0.1% solution and $0.88 \times \dot{\gamma}^{0.62}$ for the 0.4%. Importantly, Wi is greater than unity for shear rates greater than $1\,\mathrm{s}^{-1}$ (for the 0.4% solution) or $10\,\mathrm{s}^{-1}$ (for the 0.1% solution), so that we expect elasticity to dominate the flow properties at higher shear rates.

According to the criterion proposed by Mc Kinley *et al.*,[11] one expects that in the cone and plate geometry, elastic instabilities appear for $\mathrm{Wi} > M/(2\sin\theta)^{1/2}$, where the constant M usually depends on the flow curve but is about a few units. Though it is rather difficult to know with good precision the onset of the instabilities, we estimate from the observation of stress fluctuations that above $50\,\mathrm{s}^{-1}$, the flow is unstable. This is consistent with a value of M which is about 2 for the 0.1% solution and 4 for the 0.4% solution. A major consequence of these instabilities is that they can significantly contribute to the measured shear stress.[5,30] Therefore, we think we cannot trust at high shear rates the experimental flow curves displayed in Fig. 2, and the deviation from the power law function observed for the 0.1% solution is likely to be due to these elastic instabilities.

III. REFERENCE FLOW FOR SHEAR-THINNING LIQUIDS

In this section, we present numerical results obtained for a shear-thinning liquid. Solving the flow of a viscoelastic shear-thinning fluid would be very costly in terms of processing time in the studied geometry. We restrict ourselves to an oversimplified approach where elasticity is neglected and where the geometry of the flow is idealized as a network of straight channels. These simulations results aim to serve as a reference and are not intended to account for the experimental results. Simulations will then be used to interpret the experimental results, and, importantly, to account for the consequences of the disorder of the porous network. For the sake of simplicity, the liquid viscosity is approximated by a power-law, in agreement with the polymer solution properties measured in the range of flow rates studied.

A. Numerical method

We performed flow simulations using pore network modeling. This numerical approach consists of modeling the porous geometry by a network of connected channels. Such an approach is therefore well adapted to the geometry of the micromodel: it is straightforward to study in the simulations the same geometry as in the experiments.

As in the experiments, we use a square lattice of channels of uniform height h and length l, and of heterogeneous width w_{ij} (see Fig. 3), randomly generated according to a log-normal distribution of mean value w and of standard variation ϵw. All the calculations are made on a 50×50 lattice, but the results are averaged on 50 different random networks. At each node of the network, mass conservation means that for a given node i

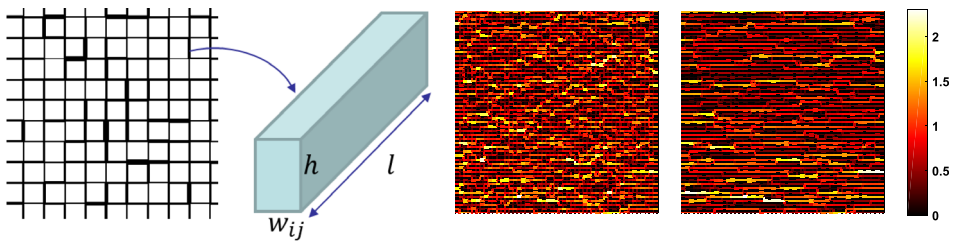

FIG. 3. *Top*: Principle of the simulation: the porous domain is idealized by a network of rectangular channels having heterogeneous widths w_{ij} of relative standard deviations ϵ. The flow rate/pressure drop relation of a power-law fluid in a rectangular channel is solved in each channel. *Bottom:* Examples of simulation results: flow rates maps, the highest flow rate are the brightest. *Left:* Newtonian fluid ($n = 1$) in a heterogeneous network ($\epsilon = 0.33$) of 50×50 nodes. *Right:* Shear-thinning fluid ($n = 0.2$). In the color bar, flow rates have been normalized by the total flow rate divided by 50.

$$\sum_j q_{ij} = 0, \tag{1}$$

where the summation is made on the neighboring nodes. The flow rate q_{ij} in channel ij is assumed to be given by the laminar fully developed channel flow of a power-law fluid. Since no analytical solution could be obtained in rectangular ducts, we use the following empiric expression proposed by Hartnett and Kostic[31] to correlate their numerical results

$$q_{ij} = \frac{\text{sign}(p_i - p_j)h^{3+\frac{1}{n}}}{4\alpha(1+\alpha)(b+a/n)}\left(\frac{|p_i - p_j|}{2Kl(1+\alpha)}\right)^{\frac{1}{n}}, \tag{2}$$

where $\alpha = h/w_{ij}$ is the aspect ratio, p_i is the pressure at node i, K, and n are the parameters involved in the power-law function $\sigma = K\dot{\gamma}^n$. In this expression, a and b are numerical constants that depend on the aspect ratio.[32]

The system of Equation (1) coupled to uniform pressure at the inlet and at the outlet as boundary conditions is solved using the Levenberg-Marquardt solver of matlab. The main approximations in this numerical approach consist in neglecting the influence of the nodes of the network and of the end effects in the channels.

Figure 3 displays typical outputs of the computation: a map of the flow rates in all of the channels of the network. Clearly, there is a strong coupling between shear-thinning and the network disorder: as compared to the Newtonian case, the flow of a shear-thinning fluid is concentrated in the channels that are parallel to the flow. The effective tortuosity of the porous medium is lowered.

B. Global pressure drop

In the experiments, we measure systematically the pressure drop as a function of the flow rate. The raw data are rather difficult to interpret for a non-Newtonian liquid as the flow properties could be shear-rate dependent. We propose to calculate from the pressure/flow rate relation an effective shear stress/shear rate relation, so that it is then possible to compare directly with rheograms. The procedure is however not straightforward since, for a given global flow rate, the mean shear rate and shear stress depend on both the network disorder and the fluid flow properties. We detail below the methodology used.

We used two different micromodels: the first one is an array of $N = 40$ parallel straight and identical rectangular channels, and the second one is an heterogeneous network of channels of similar dimensions. The first one is studied as a reference.

In the experiment, we measure the pressure drop ΔP_0 as a function of the flow rate Q_0. In the channel array device, the procedure to derive wall the shear rate $\dot{\gamma}_{w_0}$ and shear stress σ_{w_0} from these measurements is available in the literature.[33] They are given by

$$\sigma_{w_0} = \frac{\Delta P_0 hw}{2L(w+h)}, \tag{3a}$$

$$\dot{\gamma}_{w_0} = \frac{4Q_0}{Nw^2h}\left(1+\frac{w}{h}\right)\left(b+\frac{a}{n}\right), \tag{3b}$$

where N is the number of channels, L is the channel length, and a and b are the same empirical constants appearing in Equation (2); they depend on n and on the channel aspect ratio.

The case of the porous medium micromodel is much more complex: the previous relations are only correct in the case of a homogeneous network, but need to be updated for a heterogeneous structure. For real rocks, the usual procedure consists of determining the apparent viscosity using Darcy's law, taking advantage of a characteristic length scale of the rock to define an apparent shear rate.[15,34] This length is typically $\sqrt{k\phi}$, where k is the permeability and ϕ the porosity. However, such procedures lead to a shift in the shear rate, when comparing to bulk

rheograms.[34] This shift factor is found to depend on both the rock and on the fluid. This is not surprising as even for a simple channel flow, Equation (3b) reveals that the shear rate correction depends on geometry and on the power-law exponent. Furthermore, it has been shown using pore-network simulations that the tortuosity of the network is an important parameter affecting this correction,[35] due to some complex cooperative effects.[36] One can thus anticipate that Equation (3b) is not valid in heterogeneous channel networks and that a correction factor which should depend on the network heterogeneity is needed to obtain a rheogram and compare the results to the bulk rheology.

We take advantage of pore-network simulations to calculate this correction factor. When varying the network heterogeneity in the simulations, we find that the effective permeability of the media, defined as $k = S\Delta P/Q\eta$, decreases when the standard deviation of the heterogeneous channel widths is increased. In Fig. 4(a), the permeability of the network normalized by the one of a homogeneous one is shown for various network disorders and power-law exponents of the shear thinning liquid. One sees that this permeability reduction is more important for a shear-thinning fluid than for a Newtonian one, e.g., the permeability is decreased by a factor of 2 in a network of standard deviation $\epsilon = 0.45$ for a power-law fluid of exponent 0.2, but only by 20% for a Newtonian fluid. This result has an important consequence: the effective viscosity of a shear-thinning fluid depends on the size heterogeneity of the medium and cannot be directly measured using Darcy law. We take advantage of pore-network simulations to calculate this correction factor. When varying the network heterogeneity in the simulations, we find that the effective permeability of the media, defined as $k = S\Delta P/Q\eta$, decreases when the standard deviation of the heterogeneous channel widths is increased. In Fig. 4(a), the permeability of the network normalized by the one of a homogeneous one is shown for various network disorders and power-law exponents of the shear thinning liquid. One sees that this permeability reduction

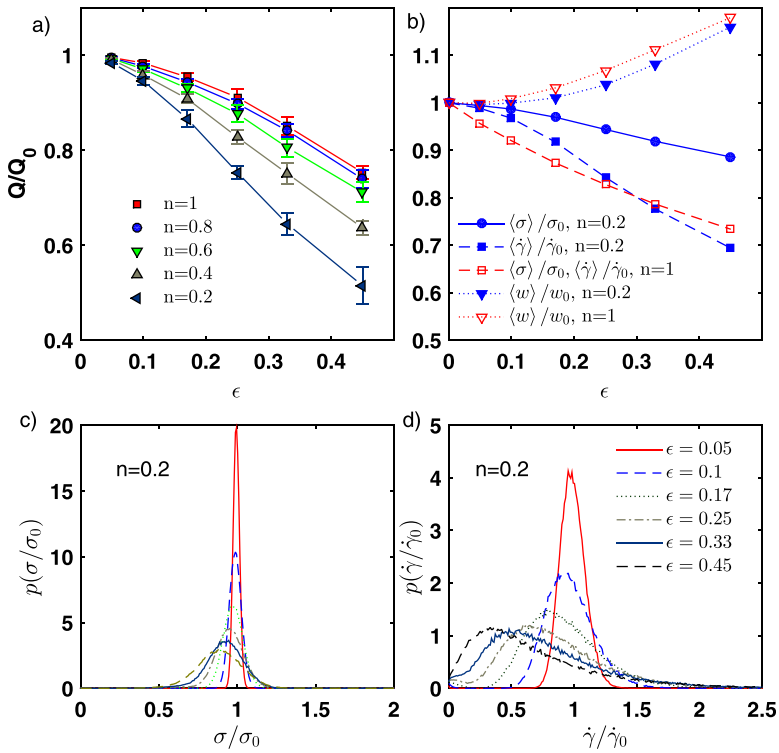

FIG. 4. Simulation results. (a) Effect of network heterogeneity ϵ and shear-thinning exponent n on the global flow rate. Flow rates Q are normalized by the flow rate in a homogeneous network Q_0 predicted for the same imposed pressure drop. (b) Mean values of the channel width w, the wall shear stress σ, and shear rate $\dot{\gamma}$, for $n = 1$ and $n = 0.2$ as function of the network heterogeneity. All these quantities are normalized by their values in a homogeneous network and are calculated using a flow rate weighted averaging. (c) and (d) PDF of the wall shear stress and shear rate (flow rate weighted) for $n = 0.2$.

is more important for a shear-thinning fluid than for a Newtonian one, e.g., the permeability is decreased by a factor of 2 in a network of standard deviation $\epsilon = 0.45$ for a power-law fluid of exponent 0.2, but only by 20% for a Newtonian fluid. This result has an important consequence: the effective viscosity of a shear-thinning fluid depends on the size heterogeneity of the medium and cannot be directly measured using Darcy law.

In order to better understand this effect, we compute from the simulation results the shear stress and shear rate probability density functions (PDF) in the medium. The results are shown in Figs. 4(c) and 4(d), for $n = 0.2$. The PDF are obtained by weighting each channel by its flow rate. This weighting allows the PDF and the mean values to reflect the contributions of each channel to the pressure/flow rate relation. Local shear stresses are computed according to $\sigma_{ij} = |P_i - P_j|hw_{ij}/2l(w_{ij} + h)$, which is the mean wall shear stress in a channel of rectangular cross-section.[33] In Fig. 4, local shear stresses are normalized by that in an homogeneous network, which is given by $\sigma_0 = \Delta Phw/2L(w + h)$. The apparent shear rate $\dot{\gamma}_{ij}$ in channel ij is directly computed from the rheological flow curve, i.e., $\dot{\gamma}_{ij} = \sigma_{ij}^{1/n}/K$. The standard deviation of the PDF of the shear stress is broader for heterogeneous media, as expected, and its mean value is slightly decreased. Looking at the PDF of the shear stress, the effect of network heterogeneity is striking, as the distribution functions become very large for heterogeneous network and highly shear-thinning liquids. As for the shear stress, the mean shear rate is decreased, but the effect is much more pronounced. This is clearly coming from the non-linearity of the shear rate/shear stress relation.

The mean values[37] of shear stress and shear rate have been systematically calculated and are shown in Fig. 4(b) for $n = 1$ (Newtonian fluid) and $n = 0.2$ (power-law exponent of the two solutions used experimentally in this work). The mean value of the channel width is also shown in this figure: it differs from the one imposed, because the mean values shown in Fig. 4(b) are weighted by the local flow rates. The increase in the mean width of the channels when the network heterogeneity is increased could be directly interpreted as follows: larger channels contribute to the flow more than smaller ones. This effect is not surprising. Less intuitively, we note that this effect is more important for Newtonian fluids than for the shear thinning ones. We will come back to this point in Sec. III C. The fact that the mean shear stress is slightly decreased when increasing the network disorder (about 10% for $\epsilon = 0.45$ and $n = 0.2$, but more than 25% for a Newtonian fluid in the same network) is due to the tortuosity of the medium. Despite flowing in larger channels which would increase the shear stress, the mean length L_{eff} of the streamlines is larger than the length of the porous medium L. Clearly, the tortuosity τ, defined as $\tau = L_{\text{eff}}/L$ is larger for a Newtonian fluid than for a shear thinning one. This effect could be observed qualitatively in Fig. 3, and will be discussed in Sec. III C.

From the calculated mean values of the shear rate and shear stress, we can define empirical correction factors for Equation (3b). In a heterogeneous channel network

$$\sigma_w = \alpha \frac{\Delta Phw}{2L(w + h)}, \tag{4a}$$

$$\dot{\gamma}_w = \beta \frac{4Q}{Nw^2h}\left(1 + \frac{w}{h}\right)\left(b + \frac{a}{n}\right), \tag{4b}$$

where $\alpha = \langle\sigma\rangle/\sigma_0$ and $\beta = (\langle\dot{\gamma}\rangle/\dot{\gamma}_0)(Q_0/Q)$. These correction factors depend on both the shear-thinning exponent and the network heterogeneity. For the conditions tested experimentally ($\epsilon = 0.33$ and $n = 0.2$), we find $\alpha = 0.91$ and $\beta = 1.20$. These corrections are rather small. However, we point out that the simulation results reveal two main differences between a shear-thinning fluid: as compared to a Newtonian one, the shear rates are much more heterogeneous, but the effective tortuosity is smaller.

C. Effective tortuosity

Let us analyze more closely the effective tortuosity of the medium. As will be detailed in Sec. IV, we are able to determine velocity estimations in each channel. We focus on the ratio

of the mean velocity in perpendicular channels over that in parallel channels, $v_\perp/v_\parallel$. This quantity is related to the effective tortuosity, as one can, using a crude approximation, write $\tau \simeq 1 + v_\perp/v_\parallel$.

From the numerical results, it is straightforward to calculate the ratio $v_\perp/v_\parallel$, by simple averaging. Here, we use simple ensemble averaging, without flow rate weighting, similar to the experimental analysis. Fig. 5 summarizes the results. We find that this ratio increases when increasing the network heterogeneity ϵ, as expected. More importantly and less intuitively, we find that it strongly depends on the shear-thinning exponent. It is higher for Newtonian fluids than for shear-thinning ones. This effect could be observed directly on the velocity fields displayed in Fig. 3. The flow of a shear thinning fluid is much less tortuous than that of a Newtonian fluid, and transverse channels do not contribute significantly to the global flow. In such a network, flow occurs in transverse channels due to the fact that some of them are wider than the parallel ones and thus globally lower the global hydrodynamic resistance, even with tortuous streamlines.

In order to understand the difference between shear thinning and Newtonian fluids, let us compare the sensitivity s_l of viscous loss $Q\Delta P$ with the channel length l ($s_l = \partial_l(Q\Delta P)/l$) and the sensitivity s_w with channel characteristic size w of the cross section. Using Equation (2) simplified assuming square cross sections, we find that the ratio of these sensitivities is given by $s_w/s_l = 1 + 3n$. This directly shows that the sensitivity to channel width is much higher for a Newtonian fluid than for a shear thinning fluid, and explains the variation shown in Fig. 5 of $v_\perp/v_\parallel$ with respect to the power-law exponent n of the fluid.

IV. EXPERIMENTAL RESULTS

A. Global pressure drop

Figure 6 displays the experimental results. In both geometries, the pressure is linear with respect to the flow rate for Newtonian liquids (see the inset in Fig. 6). More quantitatively, given the geometric features of the device and using Equation (3) for the channel array, we find a very good agreement between the data obtained with a Newtonian liquid and the prediction, as the viscosity $\sigma_{w_0}/\dot{\gamma}_{w_0}$ that is deduced from the experimental linear relation is within 2% the one measured with a rheometer (10 mPa s). For the porous medium micromodel, using Equation (4) with the values of α and β calculated numerically for $n = 1$ (see Section III B), $\alpha = 0.79$, $\beta = 0.93$, we deduce from the experiments a viscosity of 2.1 mPa s, which is in good agreement with the expected value of 2.3 mPa s. Thus, we obtain coherent experimental results obtained with Newtonian liquids, validating the experimental set up.

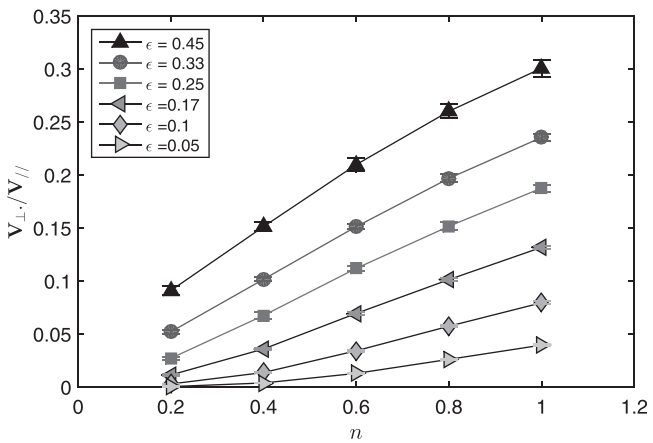

FIG. 5. Simulation results. Ratio of the mean velocity in transverse channels over that in parallel ones, for various shear-thinning exponent n and heterogeneity ϵ of the network. The calculation was made on a 50×50 grid.

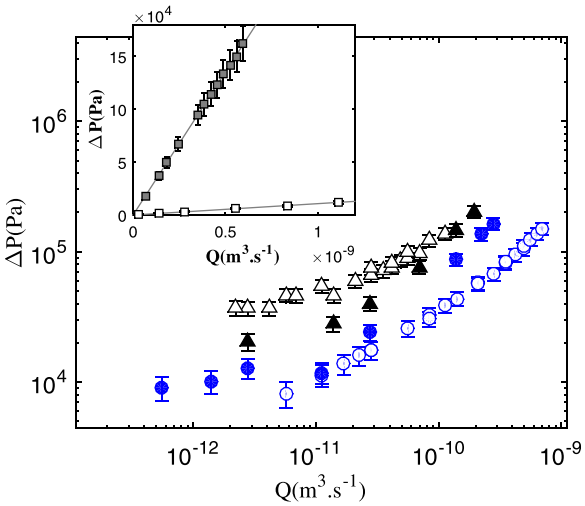

FIG. 6. Raw data of pressure drop versus applied flow rates, for different geometries and two HPAM concentrations, 0.4 wt. % (△) and 0.1 wt. % (○). The open symbols correspond to the results in straight channels, the full symbols to the results in the porous medium micromodel. In inset are shown validation experiments using Newtonian liquids: full symbols correspond to flow of isopropanol (viscosity 2.3 mPa s) in the porous medium micromodel and the open symbols to a water-glycerol mixture of viscosity 10 mPa s. For these two sets of data, best linear fits are shown and corresponds to $\Delta P = 2.71 \times 10^{14}\,Q$, and $\Delta P = 1.08 \times 10^{14}\,Q$, respectively.

The non-Newtonian results are difficult to interpret without further processing of the data. We use Equation (4) to compute the wall shear rate and shear stress from the pressure drop and flow rate empirical relation. The results obtained in the straight channel device are plotted in Fig. 7 together with the data obtained in the cone and plate geometry with the rheometer. For shear rates below $200\,s^{-1}$, both set of data are in rather good agreement. We note however that the stress in the straight channel is slightly lower in this regime than that measured in the cone and plate geometry. This effect is likely to be due to the fact that for these highly shear-thinning liquids, some specific elastic instabilities reduce the apparent viscosity.[29] These elastic instabilities appear for $\mathrm{Wi} \gtrsim 5$, i.e., for $\sigma \gtrsim 4\,\mathrm{Pa}$ for the 0.4% solution, and for $\sigma \gtrsim 1\,\mathrm{Pa}$ for the 0.1% solution.[29] Thus, in the range of shear stress tested in this work, we expect the base flow

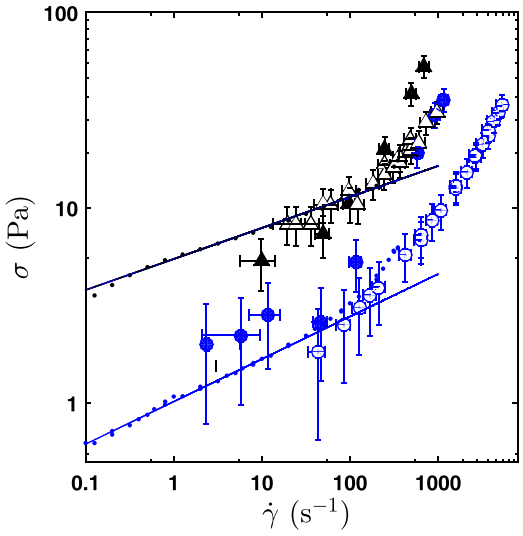

FIG. 7. Wall shear stress versus shear rate for different geometries and two HPAM concentrations, 0.4 wt. % (△) and 0.1 wt. % (○). The open symbols correspond to the results in straight channels, the full symbols to the results in the porous medium micromodel and the points to bulk rheology in cone and plate geometry.

to be unstable, except for the lowest flow rate. Slippage at the wall may also lead to a decrease of the wall shear stress, but we already reported in a previous communication with direct measurements that it is negligible in this range of shear rates.[29] In this work, we extend the above cited experiments to higher shear rates. For $\dot{\gamma}_w > 200\,\mathrm{s}^{-1}$, the wall stress deviates from the power-law dependence observed at lower shear rates in cone and plate geometry, increasing significantly. This deviation is rather difficult to interpret without additional local characterization of the flow. Indeed, at these high shear rates, even the flow in the rheometer exhibits elastic instabilities and it does not seem possible to obtain a rheometric flow and thus a characterization of the viscosity. Assuming that the power-law at lower shear rates could be extrapolated, the measurements reported in the array of straight channels in Fig. 7 indicate that, for both 0.1% and 0.4% solutions, elastic instabilities induce extra-dissipation and increase the effective viscosity of the solution in this high shear rates regime.[38] This result completes the picture drawn in Ref. 29. In a straight channel, the base laminar flow of a shear-thinning elastic fluid becomes unstable for $\mathrm{Wi} \gtrsim 5$, and the apparent viscosity is reduced due to structural homogenization over the cross section. For $\mathrm{Wi} \gtrsim 30$, the apparent viscosity increases, and this extra-dissipation is likely coming from more and more complex elastic instabilities. Indeed, we reported in Ref. 29 that the streamline perturbations evolve from single mode at $\mathrm{Wi} \sim 5$ to a much broader spectrum at $\mathrm{Wi} \sim 10$. A detailed analysis of velocity fluctuations in straight channels for $\mathrm{Wi} > 10$ would be necessary to get additional insights on this scenario, but falls out of the scope of the present article.

In Fig. 7 are also plotted the data obtained from pressure drop measurements in the heterogeneous network of straight channels. Experiments are more difficult to carry out in this device as the pressure drop stabilizes only after a rather long time at low flow rates and exhibits fluctuations at high flow rates. From the pressure drop and flow rate, we compute the effective wall shear stress and wall shear rate according to the procedure described in section III B. Two different regimes are evidenced: below $100\,\mathrm{s}^{-1}$, the shear stress measured in the heterogeneous network is similar within the data uncertainty to the one measured in the array of straight channels, and in relative agreement with the rheometric data. Above $100\,\mathrm{s}^{-1}$, the effective shear stress in the heterogeneous network increases rapidly and is much larger than in the straight channels. At $600\,\mathrm{s}^{-1}$, the shear stress (or equivalently the pressure drop) is increased by a factor of about 3, as compared to that of the straight channel. This important increase in the pressure cannot be solely due to some entrance effects, as the inlet and outlet geometries are exactly the same for both devices. The threshold above which the shear stress in the porous medium micromodel deviates from the low shear rate power-law behavior correspond to Weissenberg numbers of $\mathrm{Wi}_c = 15\ (\pm 4)$ for the 0.4% solutions and 7 (± 3) for the 0.1% solution.

As previously noted, elastic instabilities occur in straight channels at even lower Weissenberg numbers, but these have relatively small consequences:[29] at most about 30% of drag reduction and the streamlines are only slightly perturbed. The important increase of the pressure drop above Wi_c might be interpreted as due to another type of elastic instability. We performed some direct flow observations with a microscope by seeding the solution with fluorescent tracer particles, and superimpose successive images in order to get an idea of the streamlines at the local scale in the micromodel. Figure 8 shows examples of these streamlines, below and above Wi_c. The streamlines obtained below the threshold look like those for laminar flow. In contrast, the ones observed above Wi_c are clearly that of an unsteady flow as they cross each other. The motion of the tracers seems to be erratic. This proves that the flow is highly unstable, and probably turbulent, above Wi_c. Therefore, the onset of elastic instabilities coincides with the measurement of an extra-pressure drop. This does not imply that these instabilities are the only reason for this excess of pressure, as extensional viscosity for example, may contribute as the polymeric liquid flows through contractions. However, for the relatively small contractions in the studied micromodel (the relative standard deviation of channel width is 0.33), studies have shown that the corresponding extra pressure remain weak.[26,27]

It is interesting to discuss the value of Wi_c. Elastic instabilities are known to occur in curvilinear flow above a threshold given by a criterion proposed by McKinley *et al.*,[11] with $\mathrm{Wi}\sqrt{w/\mathcal{R}} > M$, where $\mathcal{R}$ is the radius of curvature of the streamlines. In the heterogeneous

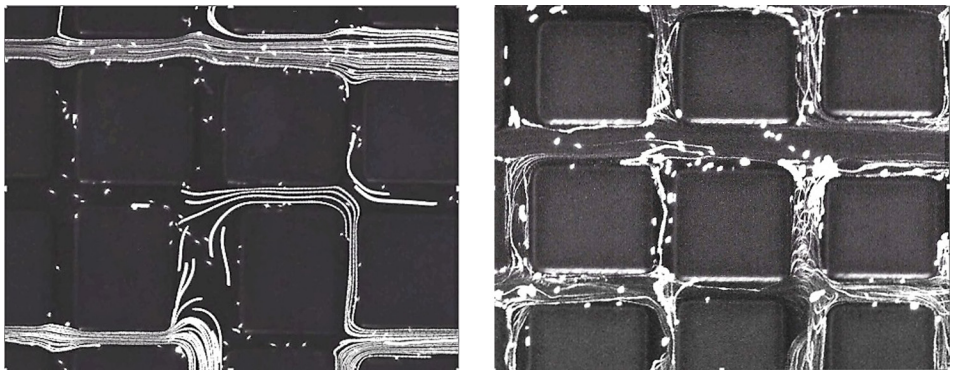

FIG. 8. Snapshots of the streamlines in the heterogeneous channel network, for the 0.4% solution. *Left:* Wi = 3. *Right:* Wi = 20. Flow direction is from the left to right.

network, we might start by assuming that the mean streamline curvature in laminar flow is of the order of $1/w$ (see, e.g., Fig. 8, left). This leads to values of M that are about 15 and 7 for the 0.4% and the 0.1%, respectively. These values are about four times those estimated from the onset of the elastic instability in the cone and plate geometry. They are also much higher than the one reported by Clarke *et al.*,[15] which are of the order of unity or below. This indicates that the effective curvature of the streamlines might be much smaller than the rough estimation used above, $1/w$. In order to match the values of M estimated in the cone and plate geometry, the curvature should be corrected by a factor of 16. This important correction might be related to the fact that the effective tortuosity of the porous media used is rather low, and that most of the streamlines of the laminar flow are straight along the channels parallel to the mean pressure gradient. As shown qualitatively in Fig. 3 and discussed in Section III C, this small effective tortuosity is specific to highly shear-thinning fluids. If this interpretation is correct, one would conclude that shear-thinning delays the onset of elastic instabilities responsible for the increase of the apparent viscosity.

Let us conclude this part by two additional remarks. First, similarly to the case of the straight channel, elastic instabilities can appear for $\mathrm{Wi} < \mathrm{Wi}_c$, without inducing extra dissipation. A local and detailed analysis of the flow is required to test this issue. Second, let us recall that the simulation results in the laminar regime reveal that the local shear rates are very widely distributed (see Fig. 4(d)), and that this large heterogeneity could greatly affect the apparent onset of the instabilities.

B. Local flow characterization

Let us now analyze in more detail the streamlines in order to get further quantitative insights of the flow above Wi_c, where elastic instabilities occur.

To do so, we took series of images and tracked fluorescent tracer particles on successive images, using standard image processing methods.[39] The experiments were carried on a Olympus IX71 equipped with a 40× objective and the images acquired by a Orca Flash 3.0 SCMOS camera. The image acquisition frequency was adjusted in order to be able to track all the particles. Fig. 9 shows an example of the particle trajectories obtained from the particle tracking procedure. We discarded trajectories that were made of less than 5 particle positions in order to remove false detections.

We restrict ourselves to the analysis and discussion the mean value of local velocities. We proceed by averaging particle displacements in the channels and dissociate channels that are parallel to the mean pressure gradient from transverse ones. For this purpose, we define regions of interest (see Fig. 9), calculate the absolute value of mean velocities in each of these regions, and average separately parallel and transverse channels. Series of 500 images were taken at about 5 different locations, in order to obtain representative mean values of the transverse and parallel velocities, designated, respectively, as $v_\perp$ and $v_\parallel$.

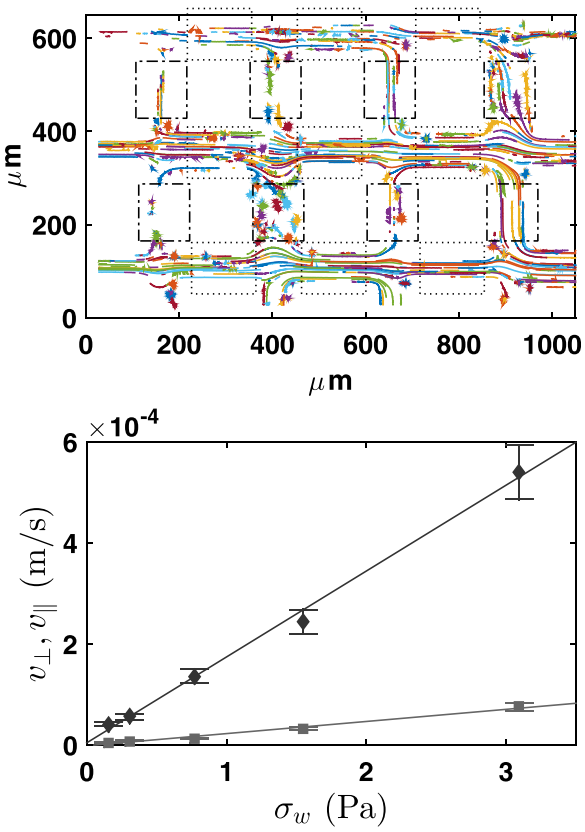

FIG. 9. *Top*: visualization of the trajectories which were tracked for a Newtonian fluid (glycerol) at 200 mbar, calculated on 500 images at 85 fps. The flow direction is from the left to the right; the dashed (respectively, dashed-dotted) rectangles illustrate the regions of the images where $v_\parallel$ (respectively, $v_\perp$) is computed. *Bottom*: Mean velocities in parallel ($v_\parallel, \diamond$) and transverse ($v_\perp, \square$) channels versus the mean wall shear stress, for a Newtonian fluids (glycerol). The data are well accounted by linear relations, and best fits lead to $v_\perp/v_\parallel = 0.14$.

The procedure is first validated using glycerol, a Newtonian fluid. As shown in Fig. 9, we find a linear relation for both parallel and transverse velocities with respect to the pressure drop. The ratio $v_\perp/v_\parallel = 0.14$ is related to the tortuosity of the porous media, it would vanish in a homogeneous channel network. In a crude approximation, the effective tortuosity can be expressed as $\tau \simeq 1 + v_\perp/v_\parallel$. The ratio $v_\perp/v_\parallel$ is also an indicator of the flow homogeneity: the greater this ratio the greater the flow in channels orientated in the unfavorable direction.

The ratio $v_\perp/v_\parallel$ has also been calculated in the simulations (see Section III C). Experiments and simulations are however in rather poor quantitative agreement, as we find for a Newtonian fluid that the ratio $v_\perp/v_\parallel$ is about 0.23 for a heterogeneity of $\epsilon = 0.33$ tested experimentally. This value is greater than the one obtained experimentally. Additional experiments using micromodels of different heterogeneity might be needed to understand this discrepancy. Despite the special care that has been taken to obtain statistically representative mean values in the experiments, let us underline that these measurements are rather complex and that some experimental bias might exist: some tracers could stick at the walls; in some channels, only a few tracers are seen; the tracers may not be uniformly distributed in the cross section, etc. Also, in the simulation, we neglect node volumes, which might be an oversimplified assumption that could lead to some bias. For these reasons, we do not focus on the difference between numerical and experimental results and restrict ourselves to commenting the variations of the ratio $v_\perp/v_\parallel$.

The experimental results for the 0.4% HPAM solution are shown in Fig. 10. At low shear stresses (below Wi_c), $v_\perp/v_\parallel$ is roughly constant and is about 0.07. This value is of the order of the one found numerically for a laminar flow (0.052). Importantly, it is half the one measured for a Newtonian fluid. We therefore find, similarly to the simulations, that in the apparent

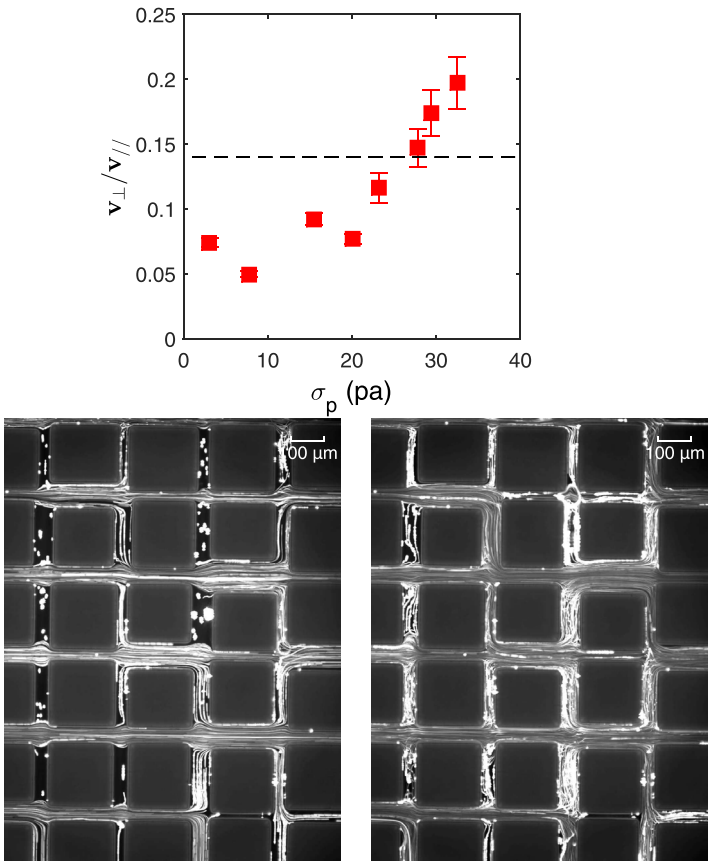

FIG. 10. Top: Ratio of velocities for 0.4 wt. % HPAM (□) and Newtonian fluid (–). In laminar flow the ratio is constant for HPAM and less important for Newtonian fluid. Beyond the onset the ratio increase and exceeds the Newtonian fluids. Bottom: Superposition of 20 successive images. Flow is from left to right. Left: $Q = 50\,\mu l/h$, $Wi = 7$. Right: $Q = 150\mu l/h$, $Wi = 15$.

"laminar" regime, the flow is less tortuous for shear thinning fluids than for Newtonian ones. When $\sigma_w > 20$ Pa, i.e., above the onset of the elastic instabilities responsible for an anomalous increase in the apparent viscosity, the value $v_\perp/v_\parallel$ is increased and even exceeds significantly the value obtained for a Newtonian fluid for $\sigma_w > 25$ Pa. This shows that elastic instabilities greatly modify the features of the flow: transverse channels, which are almost unexplored by the flow due to shear thinning, have significant flow in them above Wi_c. In fact, this flow homogenization is directly visible in the images. Fig. 10 displays examples of image superimposition taken below and above Wi_c. Some of the transverse channels that were almost at rest at low flow rates significantly contribute to the flow at higher ones.

This flow homogenization is possibly due to the fact that the effective shear stress versus shear rate relation becomes closer to that of Newtonian fluid in the high Wi regime. Though this effect could play a role, it would not explain why the value of $v_\perp/v_\parallel$ overcomes that of Newtonian fluids. Another, and to our point of view more convincing interpretation, is related to pressure fluctuations created by the elastic instabilities. In transverse channels, the flow is small because pressure gradients are small. One expects that elastic instabilities can lead to local pressure fluctuations which create important transient pressure gradients in the transverse channels. This interpretation is associated with the observation than in the unstable flow regime, some back and forth movements of tracer particles are seen in some channels. An analysis of flow fluctuations is needed to be able to support this interpretation, but falls out of the scope of this work. It is consistent with the interpretation proposed by Mitchell *et al.*, who argued that pressure fluctuations mobilize oil droplets when elastic instabilities are present.

V. CONCLUSION

In summary, we have investigated the role of elastic instabilities of shear-thinning polymer solutions in model porous media. Similarly to previous studies, we report direct experimental evidence that the flow becomes unstable above a certain threshold. Using a precise methodology to extract effective shear stress and shear rates from standard pressure-flow rate experiments, we find that the threshold is obtained for $\mathrm{Wi}_c \sim 10$, but the exact value depends on the fluid. This value is higher than previously reported using polymeric liquid with smaller shear-thinning.[15] We interpret this observation as a consequence of the fact the effective tortuosity of the porous medium studied is lower for shear-thinning fluids. Above this threshold, we find that in straight channels, the pressure drop increases significantly; but this increase is much more important in a heterogeneous network of channels.

In addition, we show that above the instability threshold, the flow of polymer solutions become more homogeneous, in the sense that flow in transverse channels is greatly enhanced. This effect can have some very important consequences. For example, in biphasic flows encountered in oil recovery or soil remediations applications, this effect might help in mobilizing trapped clusters in dead regions of the flow. As this effect reduces flow heterogeneities, it may also reduce the hydrodynamic dispersion of solutes and homogenize residence times. This could have some direct applications in heterogeneous catalysis or in analytical chemistry.

Numerical approaches which include viscoelasticity would be of high interest in order to better understand the appearance and consequences of elastic instabilities in the complex geometries investigated.

Let us finally mention that, in laminar flow, the shear thinning property of polymer solutions is responsible for the opposite effect: transverse channels have less flow than Newtonian fluids. It should be interesting to test the case of shear-thinning liquids with weak elasticity, and of Boger fluids which are elastic but not shear-thinning. For this second class of liquids, we could expect that for Boger fluids the elastic instabilities could homogenize more efficiently the flow than for shear-thinning elastic fluids.

[1]L. W. Lake, *Enhanced Oil Recovery* (Prentice-Hall, 1989).
[2]K. S. Sorbie, *Polymer-Improved Oil Recovery* (Springer Science + Business Media, New York, 1991).
[3]C. Cottin, H. Bodiguel, and A. Colin, Phys. Rev. E **82**, 046315 (2010).
[4]J. Beaumont, H. Bodiguel, and A. Colin, Soft Matter **9**, 10174 (2013).
[5]A. M. Howe, A. Clarke, and D. Giernalczyk, Soft Matter **11**, 6419 (2015).
[6]H. A. Barnes, J. Non-Newtonian Fluid Mech. **56**, 221 (1995).
[7]A. Omari, M. Moan, and G. Chauveteau, Rheol. Acta **28**, 520 (1989).
[8]A. Cuenca and H. Bodiguel, Phys. Rev. Lett. **108**, 108304 (2013).
[9]R. Larson, Rheol. Acta **31**, 213 (1992).
[10]E. S. Shaqfeh, Annu. Rev. Fluid Mech. **28**, 129 (1996).
[11]G. H. McKinley, P. Pakdel, and A. Öztekin, J. Non-Newtonian Fluid Mech. **67**, 19 (1996).
[12]J. Zilz, R. J. Poole, M. A. Alves, D. Bartolo, B. Levache, and A. Linder, J. Fluid Mech. **712**, 203 (2012).
[13]A. Groisman and V. Steinberg, Nature **405**, 53 (2000).
[14]M. Grilli, A. Vázquez-Quesada, and M. Ellero, Phys. Rev. Lett. **110**, 174501 (2013).
[15]A. Clarke, A. M. Howe, J. Mitchell, J. Staniland, L. Hawkes, and K. Leeper, Soft Matter **11**, 3536 (2015).
[16]C. Scholz, F. Wirner, J. R. Gomez-Solano, and C. Bechinger, EPL **107**, 54003 (2014).
[17]C. L. Perrin, P. M. Tardy, K. S. Sorbie, and J. C. Crawshaw, J. Colloid Interface Sci. **295**, 542 (2006).
[18]M. A. Nilsson, R. Kulkarni, L. Gerberich, R. Hammond, R. Singh, E. Baumhoff, and J. P. Rothstein, J. Non-Newtonian Fluid Mech. **202**, 112 (2013).
[19]D. Wang, J. Cheng, W. Gong, Q. Yang, Q. Li, and F. Chen, in *SPE Annual Technical Conference and Exhibition* (2000), p. SPE63227.
[20]H. Z. Dong, S. F. Fang, D. M. Wang, J. Y. Wang, Z. Liu, and W. H. Hong, in *SPE Symposium on Improved Oil Recovery* (2008), p. SPE 114342.
[21]J. Mitchell, K. Lyons, A. M. Howe, and A. Clarke, Soft Matter **12**, 460 (2016).
[22]N. Gaitonde and S. Middleman, Ind. Eng. Chem. Fundam. **6**, 145 (1966).
[23]R. Marshall and A. B. Metzner, Ind. Eng. Chem. Fundam. **6**, 393 (1967).
[24]E. Wissler, Ind. Eng. Chem. Fundam. **10**, 411 (1971).
[25]J. Deiber and W. Schowalter, "Modeling the flow of viscoelastic fluids through porous media," AIChe J. **27**, 912 (1981).
[26]J. P. Rothstein and G. H. McKinley, J. Non-Newtonian Fluid Mech. **98**, 33 (2001).
[27]F. J. Galindo-Rosales, L. Campo-Deano, F. T. Pinho, E. van Bokhorst, P. J. Hamersma, M. S. N. Oliveira, and M. A. Alves, Microfluid. Nanofluid. **12**, 485 (2012).
[28]T. Sochi, J. Polym. Sci., Part B **48**, 2437 (2010).
[29]H. Bodiguel, J. Beaumont, A. Machado, L. Martinie, H. Kellay, and A. Colin, Phys. Rev. Lett. **114**, 028302 (2015).

[30]J. Beaumont, N. Louvet, T. Divoux, M.-A. Fardin, H. Bodiguel, S. Lerouge, S. Manneville, and A. Colin, Soft Matter **9**, 735 (2013).
[31]J. Hartnett and M. Kostic, Adv. Heat Transfer **19**, 247 (1989).
[32]The following polynomial functions could be used as an approximation of the value of a and b (for $\alpha > 1$): $a = 0.1879\alpha^{-4} - 0.8097\alpha^{-3} + 1.335\alpha^{-2} - 1.002\alpha^{-1} + 0.5$; $b = 0.2913\alpha^{-4} - 0.8987\alpha^{-3} + 1.2787\alpha^{-2} - 0.9917\alpha^{-1} + 1$.
[33]Y. Son, Polymer **48**, 632 (2007).
[34]X. Lopez, P. Valvatne, and M. Blunt, J. Colloid Interface Sci. **264**, 256 (2003).
[35]J. Pearson and P. Tardy, J. Non-Newtonian Fluid Mech. **102**, 447 (2002).
[36]K. Sorbie, P. Clifford, and E. Jones, J. Colloid Interface Sci. **130**, 508 (1989).
[37]Similarly to PDF, mean values are obtained by weighting each channel by its flow rate.
[38]Reynolds numbers remain small over the whole range of flow rates studied, the largest would about 0.5 for the 0.1% solution at 7000 s^{-1} if one assumes that the power law holds at these shear rates. Inertia is thus negligible.
[39]J. C. Crocker and D. G. Grier, J. Colloid Interface Sci. **179**, 298 (1996).